

The Gemini NICI Planet-Finding Campaign: Discovery of a Close Substellar Companion to the Young Debris Disk Star PZ Tel ¹

Beth A. Biller^{1,2}, Michael C. Liu¹, Zahed Wahhaj¹, Eric L. Nielsen³, Laird M. Close³, Trent J. Dupuy¹, Thomas L. Hayward⁴, Adam Burrows⁵, Mark Chun⁶, Christ Ftaclas¹, Fraser Clarke⁷, Markus Hartung⁴, Jared Males³, I. Neill Reid⁸, Evgenya L. Shkolnik⁹, Andrew Skemer³, Matthias Tecza⁷, Niranjan Thatte⁷, Silvia H.P. Alencar¹⁰, Pawel Artymowicz¹¹, Alan Boss⁹, Elisabete de Gouveia Dal Pino¹², Jane Gregorio-Hetem¹², Shigeru Ida¹³, Marc J. Kuchner¹⁴, Douglas Lin¹⁵, Douglas Toomey¹⁶

ABSTRACT

We report the discovery of a tight substellar companion to the young solar analog PZ Tel, a member of the β Pic moving group observed with high contrast adaptive optics imaging as part of the Gemini NICI Planet-Finding Campaign. The companion

¹Institute for Astronomy, University of Hawaii, 2680 Woodlawn Drive, Honolulu, HI 96822

²Hubble Fellow

³Steward Observatory, University of Arizona, 933 North Cherry Avenue, Tucson, AZ 85721

⁴Gemini Observatory, Southern Operations Center, c/o AURA, Casilla 603, La Serena, Chile

⁵Department of Astrophysical Sciences, Peyton Hall, Princeton University, Princeton, NJ 08544

⁶Institute for Astronomy, 640 North Aohoku Place, #209, Hilo, Hawaii 96720-2700 USA

⁷Department of Astronomy, University of Oxford, DWB, Keble Road, Oxford OX1 3RH, U.K.

⁸Space Telescope Science Institute, 3700 San Martin Drive, Baltimore, MD 21218

⁹Department of Terrestrial Magnetism, Carnegie Institution of Washington, 5241 Broad Branch Road, NW, Washington, DC 20015

¹⁰Departamento de Fisica - ICEX - Universidade Federal de Minas Gerais, Av. Antonio Carlos, 6627, 30270-901, Belo Horizonte, MG, Brazil

¹¹University of Toronto at Scarborough, 1265 Military Trail, Toronto, Ontario M1C 1A4, Canada

¹²Universidade de Sao Paulo, IAG/USP, Departamento de Astronomia, Rua do Matao, 1226, 05508-900, Sao Paulo, SP, Brazil

¹³Tokyo Institute of Technology, Ookayama, Meguro-ku, Tokyo 152-8551, Japan

¹⁴NASA Goddard Space Flight Center, Exoplanets and Stellar Astrophysics Laboratory, Greenbelt, MD 20771

¹⁵Department of Astronomy and Astrophysics, University of California, Santa Cruz, CA 95064

¹⁶Mauna Kea Infrared, LLC, 21 Pookela St., Hilo, HI 96720

was detected at a projected separation of 16.4 ± 1.0 AU ($0.33 \pm 0.01''$) in April 2009. Second-epoch observations in May 2010 demonstrate that the companion is physically associated and shows significant orbital motion. Monte Carlo modeling constrains the orbit of PZ Tel B to eccentricities >0.6 . The near-IR colors of PZ Tel B indicate a spectral type of $M7 \pm 2$ and thus this object will be a new benchmark companion for studies of ultracool, low-gravity photospheres. Adopting an age of 12_{-4}^{+8} Myr for the system, we estimate a mass of $36 \pm 6 M_{\text{Jup}}$ based on the Lyon/DUSTY evolutionary models. PZ Tel B is one of few young substellar companions directly imaged at orbital separations similar to those of giant planets in our own solar system. Additionally, the primary star PZ Tel A shows a $70 \mu\text{m}$ emission excess, evidence for a significant quantity of circumstellar dust that has not been disrupted by the orbital motion of the companion.

Subject headings: brown dwarfs – planetary systems – stars: pre-main sequence

1. Introduction

High contrast imaging has recently yielded the first direct images of young extrasolar planets (Marois et al. 2008; Kalas et al. 2008; Lafrenière et al. 2008; Lagrange et al. 2009) and a number of other substellar companions (Chauvin et al. 2005; Itoh et al. 2005; Luhman et al. 2006; Schmidt et al. 2008; Thalmann et al. 2009), largely at separations >50 AU. Only a handful of substellar or planetary mass companions have been found at separations <20 AU, including the recently confirmed planet imaged around β Pic (Lagrange et al. 2010) and a few substellar companions around older (\gtrsim Gyr) stars (e.g., HR 7672 B [Liu et al. 2002]; SCR 1845-6357AB [Biller et al. 2006]).

The Near-Infrared Coronagraphic Imager (NICI) at the 8.1-m Gemini-South Telescope (Chun et al. 2008) is a dedicated AO instrument tailored expressly for direct imaging of brown dwarf and exoplanet companions. NICI combines several techniques to attenuate starlight and suppress speckles for direct detection of faint companions to bright stars: (1) Lyot coronagraphy, (2) dual-channel imaging for Spectral Differential Imaging (SDI; Racine et al. 1999; Marois et al. 2005; Close et al. 2005; Biller et al. 2007) and (3) operation in a fixed Cassegrain rotator mode for Angular Differential Imaging (ADI; Liu 2004; Marois et al. 2006; Lafrenière et al. 2007b; Biller et al. 2008). While these techniques have been used individually in large planet-finding surveys (Biller et al. 2007;

¹Based on observations obtained at the Gemini Observatory, which is operated by the Association of Universities for Research in Astronomy, Inc., under a cooperative agreement with the NSF on behalf of the Gemini partnership: the National Science Foundation (United States), the Science and Technology Facilities Council (United Kingdom), the National Research Council (Canada), CONICYT (Chile), the Australian Research Council (Australia), Ministério da Ciência e Tecnologia (Brazil) and Ministerio de Ciencia, Tecnología e Innovación Productiva (Argentina).

Lafrenière et al. 2007a; Nielsen & Close 2010), the NICI Campaign is the first time ADI and SDI have been employed simultaneously in a large survey.

Since December 2008, the NICI Planet-Finding Campaign (Liu et al. 2009) has been obtaining deep, high-contrast adaptive optics (AO) imaging of a carefully selected sample of ~ 300 young, nearby stars. We report the discovery of a close substellar companion to PZ Tel, a young solar analog (K0 spectral type) and a member of the ~ 12 Myr β Pic moving group (Zuckerman et al. 2001) with a Hipparcos distance of 51.5 ± 2.6 pc (van Leeuwen 2007).

2. Observations and Data Reduction

The NICI Campaign uses specialized observing strategies to exploit the unique capabilities of the NICI instrument. While SDI provides significant contrast gains even for non-methanated objects at separations down to $0.7''$, at $\sim 0.3''$ PZ Tel B is significantly self-subtracted in our SDI data reductions. Thus, in this letter we focus solely on ADI-based techniques. For ADI, the image rotator is turned off, and the field is allowed to rotate with the parallactic angle on the sky. The image of a true companion will rotate with the parallactic angle, while speckles will stay fixed relative to the detector. A PSF for the primary star can be built and subtracted from each frame to remove the speckle pattern.

2.1. First and Second Epoch ADI + SDI Observations

We obtained ADI and SDI observations of PZ Tel on 11 April 2009 (UT) and 9 May 2010 (UT). These observations were conducted using a flat-topped Gaussian profile focal plane mask with HWHM= $0.32''$ (referred to hereafter as the $0.32''$ mask), the CH₄ 4% Short filter ($\lambda_{central} = 1.578 \mu\text{m}$) in the blue channel, and the CH₄ 4% Long filter ($\lambda_{central} = 1.652 \mu\text{m}$) in the red channel. At each epoch, we acquired 45 1-minute frames in a combined ADI + SDI mode, over 16.7° of field rotation in epoch 1 and 23.2° in epoch 2.

Data for each camera were dark-subtracted, flat-fielded, and distortion-corrected. Sky background was negligible compared to halo brightness at the companion location and has not been removed. The focal plane mask is not completely opaque at its center, leaving an attenuated, unsaturated image of the primary star (henceforth “starspot”) which we use for image registration. Images from both channels were registered to the first blue channel image according to starspot centroid positions. To increase our sensitivity to non-methanated companions, we performed a “broadband ADI-only” reduction by combining red and blue channel images instead of subtracting them. The median combination of all the images was subtracted from each individual image to remove the light from the primary star. Individual images were then rotated and stacked.

2.2. 0.22" Mask JHKs Observations

NICI coronagraphic observations using the narrower flat-topped Gaussian focal plane mask with HWHM=0.22" (hereafter 0.22" mask) were acquired in dual-channel mode at H -band and K_s -band on 9 May 2010 UT and in single channel mode at J -band on 10 May 2010 UT. The NICI filters are on the Mauna Kea Observatories photometric system (Simons & Tokunaga 2002; Tokunaga & Vacca 2005). We acquired 10 60-s frames in each filter with the rotator on. Frames were dark-subtracted, flat-fielded, and stacked according to starspot centroid position. The DC level calculated in an annulus far from the object was subtracted to remove sky background. JHK_s -band images are presented in Fig. 1.

The 0.22" mask has an approximately Gaussian transmission profile, an inner flat plateau of 0.12" radius, and an outer cutoff of 0.4" radius. With its separation of $\sim 0.3''$, PZ Tel B is lightly attenuated by the mask. Thus we must determine the mask transmission at both the center and at the companion's position in order to measure the companion's flux ratio relative to the primary. To measure the transmission as a function of radius, we acquired JHK_s -band images of a 2MASS-selected 4.4" binary star. For each filter, the primary component was scanned across the mask along the same angular trajectory as PZ Tel B. Scans were begun with the primary under the starspot in order to accurately determine the mask center position. Images were taken at 0.02" steps out to 0.5". Integration times were chosen to keep both components unsaturated. We measured the flux ratio of the primary to the secondary as a function of the primary star displacement from the mask center using photometric apertures of 1 to 3 pixels in radius. For each photometry aperture, we fit a polynomial power-law to the mask transmission as a function of radius assuming a perfectly transparent mask beyond 0.43" radius. We used this fit to correct the measured flux ratio of PZ Tel B. At a separation of 0.33", we estimate an error in our calibration of the mask transmission of 6%, 3%, and 11% in J , H , and K_s respectively. These mask calibration errors are included in the final photometry errors.

2.3. Maskless Narrow-band ADI Observations

To acquire photometry and astrometry without attenuation due to the focal plane mask, we acquired 43 maskless narrow-band ADI images on 10 May 2010 UT. Each image had an integration time of 30.4 s, and the field rotated by 25.7° over the entire observation. The narrow-band CH₄ 1% Short filter ($\lambda_{central} = 1.587 \mu\text{m}$) was used in the red channel and the H₂ 2-1 narrow-band filter ($\lambda_{central} = 2.1239 \mu\text{m}$, width of 1.23%) was used in the blue channel. Data from each filter were reduced in separate ADI reductions (§ 2.1).

To correct losses due to self-subtraction from ADI (e.g. Marois et al. 2006) and to determine the photometric and astrometric uncertainties, we inserted simulated objects into each individual frame by scaling a cutout of the stellar peak and shifting it into position. Objects were simulated at a separation of 0.36", at position angles of 0, 180, and 270° (counterclockwise from north), and

with $\Delta\text{mag} = 4.6\text{--}5.8$ in steps of 0.1 mag. Objects were retrieved using apertures of 1–3 pixels in radius to determine self-subtraction as a function of magnitude.

3. Results

3.1. Astrometric Confirmation

Astrometric measurements are presented in Table 1. First-epoch astrometry was measured from the companion centroid position relative to the starspot under the $0.3''$ mask in the “broadband ADI-only” reduction. The companion and starspot positions were measured in each frame, with the companion detected at $S/N > 10$ per frame. Because the companion falls on a slightly different part of the $0.3''$ mask in each image, angular asymmetries in the mask transmission can cause systematic astrometric trends of up to one pixel. Thus, we adopt conservative errors on our first-epoch astrometry based on the amplitudes of these trends. During acceptance testing, the NICI platescale was measured at 18 mas/pixel.

For the second-epoch astrometry, we used the maskless ADI narrow-band dataset, measuring the centroid position of the companion relative to the unsaturated stellar peak in the final stacked image. The error was estimated from the astrometric rms scatter of the 3 simulated objects (§ 2.3) with Δmag that best matched the observed object flux. Astrometric measurements from the $0.22''$ mask broadband and the $0.3''$ mask ASDI datasets yielded similar results. We adopt the direct ADI results to avoid uncertainties from the mask transmission calibration.

In Fig. 2, we plot the measured astrometry as well as the expected motion if PZ Tel B were a background star at infinite distance, given the first epoch position and known proper and parallactic motion of the primary star. The motion of PZ Tel B over 13 months deviates from the background ephemeris at the 8.9σ level. Astrometry from the $0.3''$ mask ASDI datasets for a fainter object $\sim 3.8''$ away from PZ Tel are also shown in Fig. 2. The relative motion for this other object changes as expected for a background object, confirming that published proper motion and parallax of the primary star combined with the astrometric calibration of NICI are accurate.

We reduced archival VLT NACO data of this system obtained on 22 July 2003 with the K_S -band filter and the $0.013''/\text{pixel}$ camera, originally reported in Masciadri et al. (2005). If the object detected by NICI was moving with respect to PZ Tel A as a background object, it should have had a separation of $>0.5''$ in 2003 and would have been detected at $>15\sigma$ in the VLT data. By scaling and adding a PSF star image (from an unsaturated November 2003 NACO dataset of Gl 86) to the NACO data, we estimate that PZ Tel B had a separation of $<0.17''$ in 2003.

3.2. Photometry, Mass Estimates, and Limits on Other Companions in the Field

Aperture photometry was measured from both the 0.22" mask JHK_s datasets and the direct ADI narrowband dataset using aperture sizes from 1-3 pixels in radius. Photometry results were consistent for all apertures; we adopt the 2-pixel aperture results (Table 1). As described in Section 2.3, simulated objects were inserted and retrieved to convert between measured flux and simulated Δmag and also to determine photometric errors as a function of Δmag . A JHK_S color-color diagram for PZ Tel B compared to field objects is presented in Fig. 3. While NICI photometry for PZ Tel B is reported in the MKO filter system and photometry for PZ Tel A is reported in 2MASS magnitudes, the differences between the two systems are small compared to the measurement uncertainties. PZ Tel B's measured colors are similar to mid/late-M field dwarfs.

We estimate the mass and T_{eff} of the companion based on the DUSTY models of Chabrier et al. (2000). PZ Tel B's $J - H$ color is consistent with the DUSTY model colors expected from young substellar objects at 12 and 20 Myr, so use of the DUSTY models is appropriate. Age estimates for the β Pic moving group include 12^{+8}_{-4} Myr (Zuckerman et al. 2001), 13 ± 4 Myr for the β Pic member GJ 3305 (Feigelson et al. 2006), and 11.2 Myr (Ortega et al. 2009). To account for the age range cited in the literature, we estimated the mass using a uniform distribution of ages between 8 and 20 Myr. We have chosen to work from the bolometric luminosity rather than absolute magnitudes; bolometric luminosities are less susceptible to uncertainties in the model atmospheres than single band magnitudes (Chabrier et al. 2000). Comparing to colors of field M dwarfs compiled by Leggett et al. (2010), we estimate $\text{SpT} = M7 \pm 2$ for PZ Tel B. JHK_S . Colors vary somewhat between field M dwarfs and younger objects; thus, we have placed conservative errors on our estimated spectral type. We estimate a bolometric magnitude for PZ Tel B of 10.96 ± 0.18 mag from our measured M_{K_s} and $\text{BC} = 3.1 \pm 0.1$ mag (using the K -band bolometric correction vs. spectral type relation from Golimowski et al. 2004a). We derive a model mass of $36 \pm 6 M_{\text{Jup}}$, model T_{eff} of 2702 ± 84 K and model $\log(g)$ of 4.20 ± 0.11 dex. Using the same input age grid and the single band magnitudes yielded similar mass estimates (see Figure 3, right panel). Using the same bolometric magnitude methodology with the grainless NextGen models from Baraffe et al. (1998), we derive similar values of $44 \pm 9 M_{\text{Jup}}$ and 2764 ± 67 K. Interpolating over the same age range, using our derived absolute H -band magnitude and the models of Burrows et al. (1997, 2001), we also find a similar mass range of $38 \pm 8 M_{\text{Jup}}$.

Although a few fainter background objects were seen in the PZ Tel field at separations $< 8''$, no other common proper motion companion was detected by NICI. We achieved 5σ contrast limits of 12.9 mag at 0.5", 14.6 mag at 1", and 16.6 mag at 2.25" in our $1.6\mu\text{m}$ SDI + ADI dataset. These contrast limits were verified by extensive simulated planet tests. Interpolating from the DUSTY models of Chabrier et al. (2000) and adopting an age of 12 Myr, our observations are deep enough to detect any planets with masses $\geq 6 M_{\text{Jup}}$ at separations $\geq 0.5''$.

3.3. Constraints on Orbital Parameters

We estimate the semimajor axis of PZ Tel B’s orbit from its observed separation. Assuming a uniform eccentricity distribution between $0 < e < 1$ and random viewing angles, Dupuy & Liu (2010) compute a median correction factor between projected separation and semimajor axis of $1.10_{-0.36}^{+0.91}$ (68.3% confidence limits). Using this, we derive a semimajor axis of 20_{-7}^{+18} AU for PZ Tel B based on its observed separation in May 2010. These correspond to an orbital period estimate of 79_{-21}^{+26} yr, for an assumed total system mass of $1.284_{-0.200}^{+0.050} M_{\odot}$.

We used the 2009 and 2010 NICI astrometry for PZ Tel B to place constraints on its orbital eccentricity through Monte Carlo simulations that account for astrometric errors and all possible inclinations ($0^{\circ} < i < 90^{\circ}$). For each inclination, we used 10^4 uniformly distributed values of the PA of the ascending node ($0^{\circ} < \Omega < 360^{\circ}$), allowing for different deprojections of the observed astrometry from the sky plane to the orbital plane. We computed the radial separation (r) and instantaneous velocity of PZ Tel B (v) for each possible orbital plane, using the parallax to convert to physical units. Assuming a system mass of $1.084\text{--}1.334 M_{\odot}$, we found the semimajor axis for each simulated orbit ($a = r/(2 - rv^2/M_{\text{tot}})$). By considering the amplitude of the transverse velocity of PZ Tel B in the orbital plane (v_T), we found the eccentricity corresponding to each trial ($e = \sqrt{1 - r^2 v_T^2 / a}$). In $\approx 30\%$ of cases, the trial orbits were unbound ($e \geq 1$, $a < 0$), and these were excluded from the analysis. Most of the resulting trial orbits are highly eccentric, and in Figure 4 we show the 2σ minimum allowed eccentricity as a function of the assumed inclination. Our Monte Carlo simulations effectively rule out orbits with $e < 0.6$ for any assumed inclination, due to the fact that PZ Tel B displays a large radial velocity given the known mass of the system that cannot be totally accounted for by projection effects. We choose not to assume an input distribution for inclination that would allow us to derive confidence limits on eccentricity, as randomly oriented orbits are not likely to be appropriate because of observational selection effects. (Highly eccentric companions are preferentially discovered face-on, which is the opposite sense of the geometrical preference for edge-on orbits, e.g. Dupuy & Liu 2010).

The high eccentricity may be due to a dynamical interaction with another body. However, a radial velocity measurement by Soderblom et al. (1998) rules out the possibility that PZ Tel A is a double-lined spectroscopic binary. Also, PZ Tel A shows a $70 \mu\text{m}$ emission excess (Rebull et al. 2008), evidence for a significant quantity of circumstellar dust undisrupted by the orbital motion of the companion. Assuming a simple blackbody and characteristic temperature of 41 K, Rebull et al. (2008) set a minimum radius for the inner edge of 50 AU. Artymowicz & Lubow (1994) find that binaries at a range of mass ratios and disk viscosities and with eccentricities > 0.6 will have $\frac{r_{\text{edge}}}{a} \geq 2.5$ where r_{edge} is the inner edge of the circumbinary disk and a is the semimajor axis of the binary. If the inner edge of the circumbinary disk is at 50 AU, the semimajor axis of the orbit of PZ Tel AB is likely ≤ 20 AU.

4. Conclusions

With an estimated mass of $36 \pm 6 M_{Jup}$, PZ Tel B is among the lowest-mass companions directly imaged around a young solar analog (e.g. compilation in Zuckerman & Song 2009). There are only three other planetary or substellar companions known to date in the ~ 10 Myr age range – the recently confirmed planet around β Pic (Lagrange et al. 2010), the mid-to-late L dwarf 2MASS 1207-39B in the ~ 8 Myr TW Hydra Association (Chauvin et al. 2005), and the $\sim 20 M_{Jup}$ late-M dwarf TWA 5B (Lowrance et al. 1999). PZ Tel B will be a new benchmark companion for studies of ultracool, low-gravity photospheres. The projected separation of PZ Tel B is only 18 AU, making it one of very few substellar or planetary companions directly imaged at separations of < 20 AU. Further astrometry and spectroscopy of this object will set additional limits on its orbital properties and provide improved estimates for effective temperature and surface gravity, better constraining the mass and formation history of this object.

We thank Adam Kraus for useful suggestions. B.B. was supported by Hubble Fellowship grant HST-HF-01204.01-A awarded by the Space Telescope Science Institute, which is operated by AURA for NASA, under contract NAS 5-26555. This work was supported in part by NSF grants AST-0713881 and AST-0709484. This publication makes use of data products from the Two Micron All Sky Survey, which is a joint project of the University of Massachusetts and the Infrared Processing and Analysis Center/California Institute of Technology, funded by NASA and NSF.

Facilities: Gemini-South (NICI).

REFERENCES

- Artymowicz, P., & Lubow, S. H. 1994, ApJ, 421, 651
- Baraffe, I., Chabrier, G., Allard, F., & Hauschildt, P. H. 1998, A&A, 337, 403
- Biller, B. A., Kasper, M., Close, L. M., Brandner, W., & Kellner, S. 2006, ApJ, 641, L141
- Biller, B. A., et al. 2007, ApJS, 173, 143
- Biller, B., et al. 2008, Proc. SPIE, 7015,
- Burrows, A., et al. 1997, ApJ, 491, 856
- Burrows, A., Hubbard, W. B., Lunine, J. I., & Liebert, J. 2001, Reviews of Modern Physics, 73, 719
- Chabrier, G., Baraffe, I., Allard, F., & Hauschildt, P. 2000, ApJ, 542, 464
- Chauvin, G., Lagrange, A.-M., Dumas, C., Zuckerman, B., Mouillet, D., Song, I., Beuzit, J.-L., & Lowrance, P. 2005, A&A, 438, L25

- Chiu, K., Fan, X., Leggett, S. K., Golimowski, D. A., Zheng, W., Geballe, T. R., Schneider, D. P., & Brinkmann, J. 2006, *AJ*, 131, 2722
- Chun, M., et al. 2008, *Proc. SPIE*, 7015,
- Close, L. M., et al. 2005, *Nature*, 433, 286
- D’Antona, F., & Mazzitelli, I. 1994, *ApJS*, 90, 467
- Dupuy, T. & Liu, M. 2010, *ApJ*, revised
- Feigelson, E. D., Lawson, W. A., Stark, M., Townsley, L., & Garmire, G. P. 2006, *AJ*, 131, 1730
- Geballe, T. R., et al. 2002, *ApJ*, 564, 466
- Golimowski, D. A., et al. 2004, *AJ*, 127, 3516
- Golimowski, D. A., et al. 2004, *AJ*, 128, 1733
- Itoh, Y., et al. 2005, *ApJ*, 620, 984
- Kalas, P., et al. 2008, *Science*, 322, 1345
- Knapp, G. R., et al. 2004, *AJ*, 127, 3553
- Lafrenière, D., et al. 2007, *ApJ*, 670, 1367
- Lafrenière, D., Marois, C., Doyon, R., Nadeau, D., & Artigau, É. 2007, *ApJ*, 660, 770
- Lafrenière, D., Jayawardhana, R., & van Kerkwijk, M. H. 2008, *ApJ*, 689, L153
- Lagrange, A.-M., et al. 2009, *A&A*, 493, L21
- Lagrange, A. M., et al. 2010, *Science*, in press
- Leggett, S. K., et al. 2010, *ApJ*, 710, 1627
- Liu, M. C., Fischer, D. A., Graham, J. R., Lloyd, J. P., Marcy, G. W., & Butler, R. P. 2002, *ApJ*, 571, 519
- Liu, M. C. 2004, *Science*, 305, 1442
- Liu, M. C., et al. 2009, *American Institute of Physics Conference Series*, 1094, 461
- Lowrance, P. J., et al. 1999, *ApJ*, 512, L69
- Luhman, K. L., et al. 2006, *ApJ*, 649, 894
- Marois, C., Doyon, R., Nadeau, D., Racine, R., Riopel, M., Vallée, P., & Lafrenière, D. 2005, *PASP*, 117, 745

- Marois, C., Lafrenière, D., Doyon, R., Macintosh, B., & Nadeau, D. 2006, *ApJ*, 641, 556
- Marois, C., Macintosh, B., Barman, T., Zuckerman, B., Song, I., Patience, J., Lafrenière, D., & Doyon, R. 2008, *Science*, 322, 1348
- Masciadri, E., Mundt, R., Henning, T., Alvarez, C., & Barrado y Navascués, D. 2005, *ApJ*, 625, 1004
- Nielsen, E. and Close, L. 2010, *ApJ*, in press
- Ortega, V. G., Jilinski, E., de la Reza, R., & Bazzanella, B. 2009, *AJ*, 137, 3922
- Racine, R., Walker, G. A. H., Nadeau, D., Doyon, R., & Marois, C. 1999, *PASP*, 111, 587
- Rayner, J. T., Cushing, M. C., & Vacca, W. D. 2009, *ApJS*, 185, 289
- Rebull, L. M., et al. 2008, *ApJ*, 681, 1484
- Schmidt, T. O. B., Neuhäuser, R., Seifahrt, A., Vogt, N., Bedalov, A., Helling, C., Witte, S., & Hauschildt, P. H. 2008, *A&A*, 491, 311
- Simons, D. A., & Tokunaga, A. 2002, *PASP*, 114, 169
- Soderblom, D. R., King, J. R., & Henry, T. J. 1998, *AJ*, 116, 396
- Thalmann, C., et al. 2009, *ApJ*, 707, L123
- Tokunaga, A. T., & Vacca, W. D. 2005, *PASP*, 117, 421
- van Leeuwen, F. 2007, *A&A*, 474, 653
- Zuckerman, B., & Song, I. 2009, *A&A*, 493, 1149
- Zuckerman, B., Song, I., Bessell, M. S., & Webb, R. A. 2001, *ApJ*, 562, L87

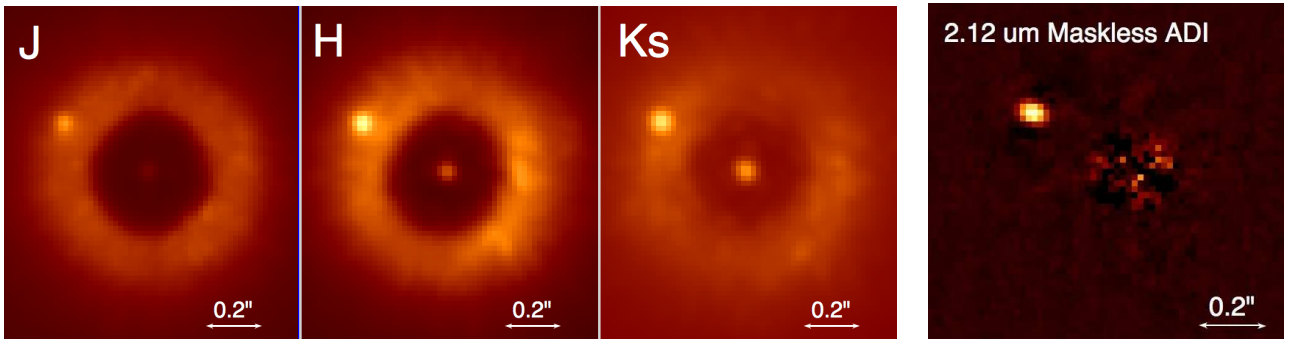


Fig. 1.— Left: J , H , and K_s -band images of the PZ Tel system obtained with NICI in direct imaging mode at the Gemini-South Telescope in May 2010. North is up, east is left. The primary resides at the center of the translucent $0.22''$ radius focal plane mask and is attenuated by a factor of 329 in J , 214 in H , and 131 in K_s -band. The confirmed companion is at $0.36''$ separation and $\text{PA}=59.4^\circ$ with flux ratios of $\Delta J = 5.40 \pm 0.13$, $\Delta H = 5.38 \pm 0.09$, and $\Delta K_s = 5.04 \pm 0.10$ mag. Right: Maskless ADI H_2 2-1 ($2.12 \mu\text{m}$) image from May 2010. Light from the primary has been removed by ADI processing.

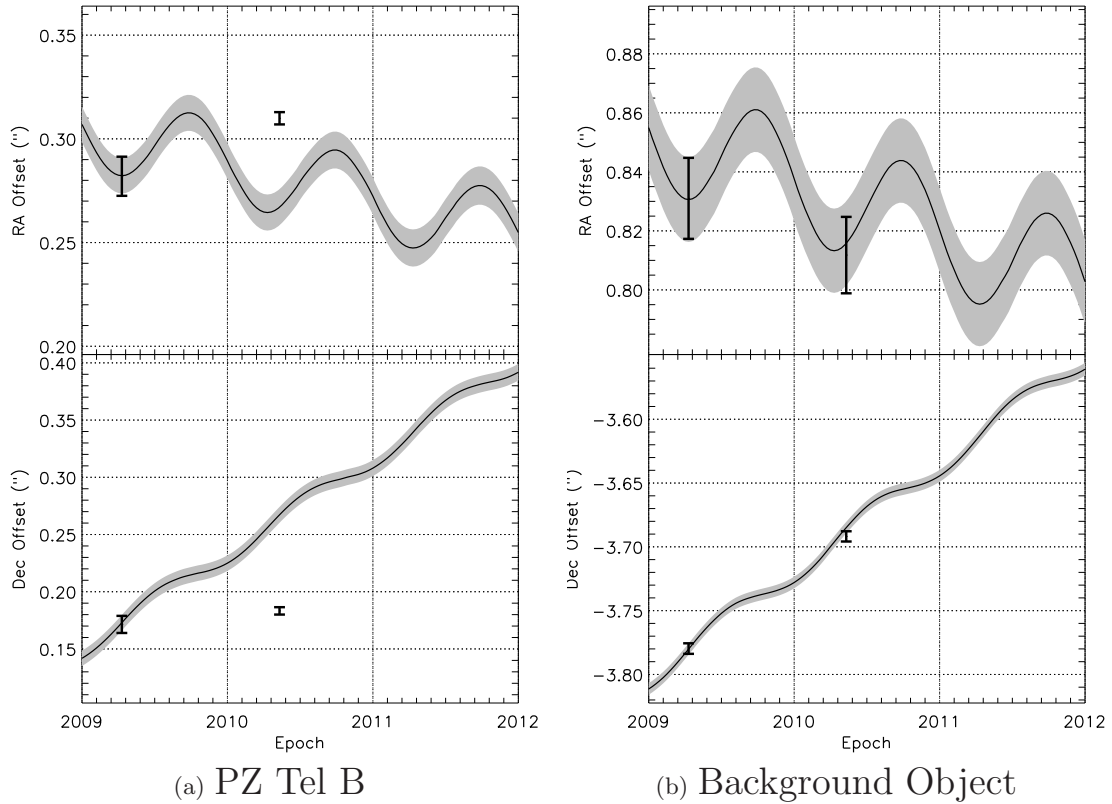


Fig. 2.— On-sky motion measured for the PZ Tel B (a) and a faint background object at $3.8''$ in the same dataset (b). The expected motion and 1σ uncertainty for a background object are overplotted, given the known proper and parallactic motion of the primary star, and the measured first-epoch position of the companion and background object. PZ Tel B cannot be a background object, as its motion diverges from the expected background track at the 8.9σ level. In contrast, the object at $3.8''$ separation moves as expected relative to the primary for a background object. Astrometry errors are measured in separation and PA relative to PZ Tel A and converted to RA and DEC. A 0.5° PA error at $3.8''$ separation translates to a considerably larger linear error than the same error at $0.33''$ separation, hence the larger error bars in RA for the background object.

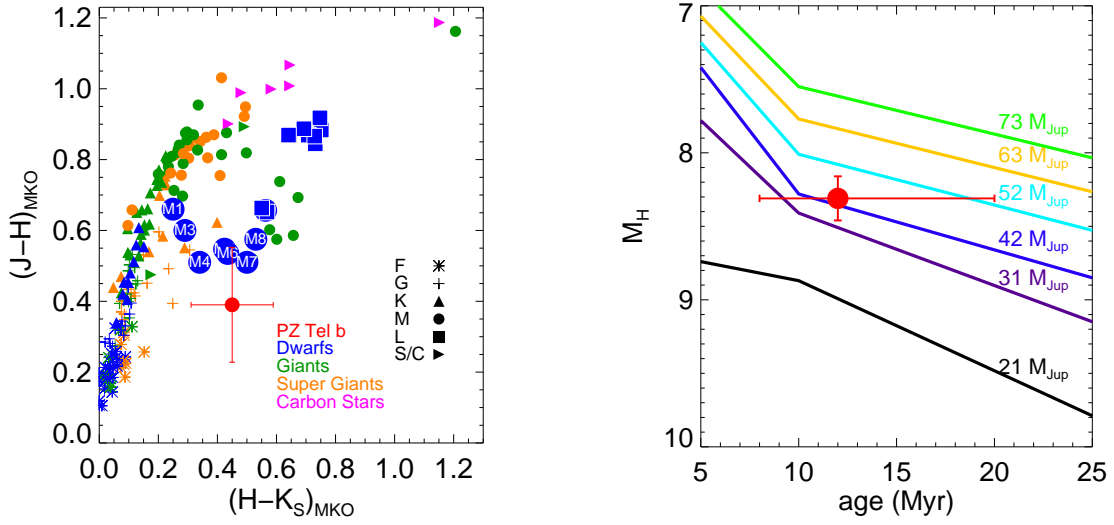


Fig. 3.— Left: the JHK_S colors of PZ Tel B compared to field objects (from Rayner et al. 2009, figure 37). The L dwarf colors are drawn from a compilation by Sandy Leggett (Leggett et al. 2010; Chiu et al. 2006; Golimowski et al. 2004b; Knapp et al. 2004; Geballe et al. 2002). PZ Tel B’s colors are plotted as a red circle and are consistent with those of a mid to late M dwarf. M dwarf points are shown as the average over several objects at each subclass. Right: M_H vs. age using DUSTY model values from Chabrier et al. (2000). PZ Tel B is plotted as a red circle.

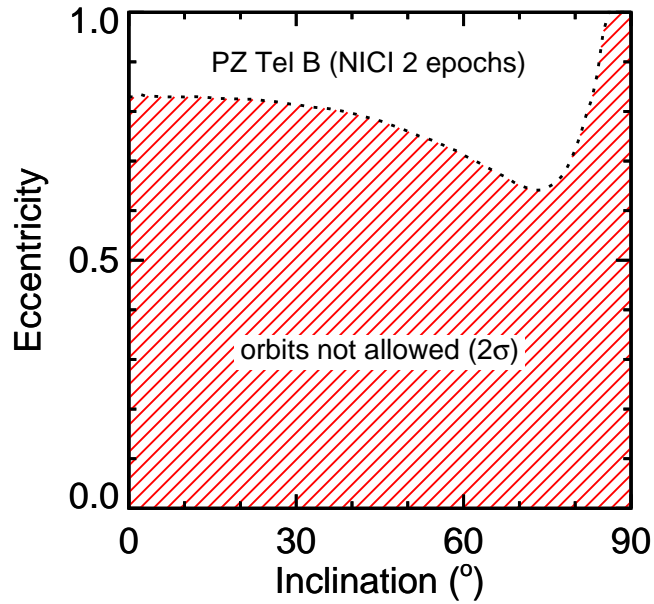


Fig. 4.— Monte Carlo constraints on inclination and eccentricity of PZ Tel B from our 2 epochs of NICI astrometry. For each inclination, 10^4 values of the PA of ascending node (Ω) were randomly drawn to allow for different deprojections of the observed astrometry from the plane of the sky to the plane of the orbit. In $\approx 30\%$ of cases, the resulting trial orbits were unbound ($e \geq 1$, $a < 0$), and these were excluded from the analysis. Most of the resulting trial orbits are highly eccentric. These results constrain the orbit of PZ Tel B to eccentricities of >0.6 .

Table 1. Properties of the PZ Tel AB System

	Primary	Secondary
Distance	51.5±2.6 pc ^a	
Age	12 ⁺⁸ ₋₄ Myr ^b	
Proper Motion (μ_α, μ_δ)	(17.6±1.1, -83.6±0.8) mas/yr ^a	
Separation: 11 Apr 2009 UT	0.330±0.010'' (16.4±1.0 AU)	
Position Angle: 11 Apr 2009 UT	59.0±1.0°	
Separation: 9 May 2010 UT	0.360±0.003'' (17.9±0.9 AU)	
Position Angle: 9 May 2010 UT	59.4±0.5°	
ΔJ (mag)	...	5.40±0.14
ΔH (mag)	...	5.38±0.09
ΔK_S (mag)	...	5.04±0.15
ΔCH_4 1% short (mag)	...	5.22±0.12
ΔH_2 1-0 (mag)	...	5.12±0.13
J (mag)	6.86±0.02 ^c	12.26±0.14
H (mag)	6.49±0.05 ^c	11.87±0.10
K_S (mag)	6.38±0.02 ^c	11.42±0.15
$J - H$ (mag)	0.37±0.05	0.39±0.17
$H - K_S$ (mag)	0.11±0.06	0.45±0.18
M_J (mag)	3.30±0.12	8.70±0.18
M_H (mag)	2.93±0.12	8.31±0.15
M_{K_s} (mag)	2.82±0.12	7.86±0.19
Spectral type	K0	[M7±2] ^d
Estimated Mass (from L_{bol})	1.25 ^{+0.05} _{-0.20} M _☉ ^e	36±6 M _{Jup}
Estimated T_{eff} (from L_{bol})	...	2702±84 K
Estimated log(g) (from L_{bol})	...	4.20±0.11 dex

^avan Leeuwen (2007)

^bZuckerman et al. (2001)

^cfrom 2MASS

^dEstimated from JHK_S colors (§ 3.2)

^eD’Antona & Mazzitelli (1994)